

AlN Thin-Film Vacuum Ultraviolet Photodetector With High Operating Temperature and High Rejection Ratio

Peixuan Zhang, Kewei Liu^{ID}, Member, IEEE, Yongxue Zhu, Qiu Ai, Zhen Cheng, Jialin Yang, Xing Chen, Binghui Li, Lei Liu, and Dezhen Shen

Abstract—AlN thin-film vacuum ultraviolet (VUV) photodetector was prepared by molecular beam epitaxy (MBE) device on $c\text{-Al}_2\text{O}_3$ substrate. By a complete surface nitridation of sapphire substrate in nitrogen plasma, the epitaxial preparation of high-quality thin AlN film was realized without any buffer layer. The AlN photodetector has an ultralow dark current (~ 40 fA at 20 V), a high VUV/ultraviolet-c (UVC) (R_{185}/R_{222}) rejection ratio ($>10^3$), a high responsivity (30 mA/W), and an ultrafast response (90%–10% decay time ~ 900 ns) at room temperature. More interestingly, an excellent temperature tolerance of the device can be observed, and there is no obvious degradation in the VUV/UVC rejection ratio and response speed with increasing the temperature from 25 °C to 500 °C. Even at 500 °C, the dark current of the device is only 218 pA at 20 V, and the responsivity can reach to 67.3 mA/W. These results indicate that the device has excellent wavelength selective detection ability and high-temperature detection ability in the VUV band, which can be attributed to the relatively high-quality AlN thin film and the avoidance of the impact of buffer layer. Our findings provide an effective way to realize high-performance AlN VUV photodetector, which can be operated in high-temperature environment.

Index Terms—AlN, high temperature, photodetector, vacuum ultraviolet (VUV).

Manuscript received 15 May 2023; revised 11 July 2023; accepted 2 August 2023. Date of publication 16 August 2023; date of current version 1 March 2024. This work was supported in part by the National Natural Science Foundation of China under Grant 62074148, Grant 11727902, and Grant 12204474; and in part by the National Ten Thousand Talent Program for Young Top-Notch Talents and Youth Innovation Promotion Association, Chinese Academy of Sciences (CAS), under Grant 2020225. The review of this article was arranged by Editor F. Medjdoub. (Corresponding author: Kewei Liu.)

Peixuan Zhang, Kewei Liu, Xing Chen, Binghui Li, Lei Liu, and Dezhen Shen are with the State Key Laboratory of Luminescence and Applications, Changchun Institute of Optics, Fine Mechanics and Physics, Chinese Academy of Sciences, Changchun 130033, China, and also with the Center of Materials Science and Optoelectronics Engineering, University of Chinese Academy of Sciences, Beijing 100049, China (e-mail: liukw@ciomp.ac.cn).

Yongxue Zhu, Qiu Ai, Zhen Cheng, and Jialin Yang are with the State Key Laboratory of Luminescence and Applications, Changchun Institute of Optics, Fine Mechanics and Physics, Chinese Academy of Sciences, Changchun 130033, China.

Color versions of one or more figures in this article are available at <https://doi.org/10.1109/TED.2023.3303126>.

Digital Object Identifier 10.1109/TED.2023.3303126

I. INTRODUCTION

HIGH-SENSITIVITY detection of vacuum ultraviolet (VUV, 120–200 nm) light has the vital significance for space science (space exploration, space physics, etc.) and radiation monitoring (synchrotron radiation, free electron laser, etc.) [1], [2], [3], [4], [5]. To meet the requirements of practical applications, the operation of photodetectors must be able to work in harsh environments of strong radiation and high temperature. Wide bandgap (WBG) semiconductor materials (such as ZnO [6], [7], [8], GaN [9], [10], [11], SiC [12], [13], [14], Ga₂O₃ [15], [16], ZnGa₂O₄ [17], and diamond [18]) have the inherent advantages of high thermal stability and high radiation resistance, which are considered to be ideal candidates for ultraviolet (UV) photodetection in harsh environments. In spite of some progress, the reported photodetectors based on WBG semiconductor cannot meet the requirements for selective and accurate detection of VUV light. This is mainly because their relatively narrow bandgaps make the devices still have strong response to the light with a wavelength longer than 200 nm. As the material with the largest bandgap (about 6.2 eV at room temperature) among III–V nitride semiconductors, AlN has good chemical stability, high mobility, high thermal conductivity (2.85 W/cm·K, about twice that of Si), and strong radiation resistance, which is very suitable for VUV detection in harsh environments [19], [20], [21], [22], [23], [24], [25].

So far, due to the lack of high-quality AlN single-crystal substrate, the reported AlN films are commonly heteroepitaxial on other substrates, including $c\text{-Al}_2\text{O}_3$ [26], [27], Si [28], GaN [29], SiC [30], and so on. Among them, $c\text{-Al}_2\text{O}_3$ is currently the most widely used AlN heteroepitaxy substrate for the VUV detection application because of its low price and excellent thermal stability, and a AlN buffer layer has been commonly utilized to obtain high-quality AlN epitaxial film. For example, Li et al. [20] prepared a VUV photodetector with metal–semiconductor–metal (MSM) structure by growing 1.5- μm -thick AlN on AlN buffer/sapphire substrate using metal–organic chemical vapor deposition (MOCVD). When the applied bias is 100 V, the peak responsivity of the device at 200 nm is 0.4 A/W. BenMoussa et al. [24] demonstrated a similar MSM VUV photodetector on AlN (thickness: 1.06 μm)/AlN buffer/sapphire by MOCVD, and the

device has an ultralow dark current of 0.2 pA (15 V) at 25 °C. However, due to the subbandgap absorption of low-quality AlN buffer layers, the VUV/ultraviolet-c (UVC) rejection ratio of such devices is generally not high. Nevertheless, due to the relatively large lattice mismatch and thermal mismatch between AlN and sapphire, obtaining high crystalline quality AlN films without buffer layers and their high-performance photodetectors still face significant challenges [31], [32].

Compared with the MOCVD technology, molecular beam epitaxy (MBE) has unique advantages in the preparation of AlN thin films (such as high vacuum growth environment, low growth temperature, and so on), so it is expected to achieve the epitaxial preparation of high-quality thin-layer AlN thin films without buffer layer. In addition, no information can be found about the AlN VUV photodetectors operating at temperature higher than 300 °C. In this work, high-quality AlN thin film was fabricated on *c*-Al₂O₃ through full nitriding technique by MBE without any buffer layer. Based on this AlN film, MSM structure photodetector has been demonstrated and investigated at various temperatures from 25 °C to 500 °C. At 25 °C, AlN photodetector has an ultralow dark current (~ 40 fA at 20 V), a high VUV/UVC rejection ratio ($R_{185}/R_{222} > 10^3$), and an ultrafast response speed (90%–10% decay time ~ 900 ns). Moreover, even at 500 °C, the dark current of the device is still only 218 pA at 20 V with a VUV/UVC rejection ratio of more than 10^3 and a responsivity of 67.3 mA/W, indicating the excellent VUV photoelectric detection ability at high temperature. The relatively high crystalline quality of AlN film and the absence of low-quality buffer layer can be responsible for the high performance of our device in a wide range of temperatures. This work provides a feasible way to prepare high-performance AlN VUV detectors that can work in harsh environment.

II. MATERIAL EPITAXY AND DEVICE FABRICATION

AlN thin film was heteroepitaxially grown on *c*-plane sapphire by MBE. 6N-pure Al obtained from a standard Knudsen effusion cell and 6N-pure N₂ activated by a radio frequency (RF) plasma source were chosen to be used as the precursors. Prior to growth, the substrate was pretreated at 700 °C for 2 h to remove gas and organic contaminants attached to the surface. After that, the substrate was nitrized completely with an RF plasma power of 350 W and a nitrogen flow rate of 1.8 sccm. Subsequently, the AlN thin film was grown at a substrate temperature of 780 °C and a chamber pressure of 1×10^{-6} Torr. The temperature of the Al source was fixed at 1180 °C, and the flow rate of N₂ was kept at 0.7 sccm with an RF power of 350 W. In situ monitoring of the film during nitriding and growth was carried out by reflection high-energy electron diffractometer (RHEED). AlN MSM photodetector with Pt interfinger electrodes was fabricated by lithography and magnetron sputtering techniques. Finally, the device was subjected to rapid thermal annealing for 10 min in Ar atmosphere at 600 °C to improve its stability.

UV spectrophotometer (Shimadzu UV-3101 PC scanning spectrophotometer), Raman shift spectrum, high-resolution X-ray diffraction (HRXRD) (Bruker D8 Discover), scanning electron microscopy (SEM) (Hitachi S-4800), and atomic

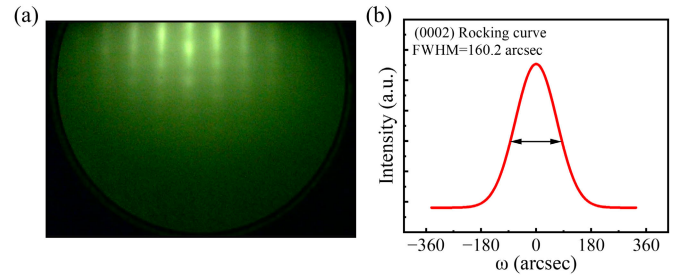


Fig. 1. (a) RHEED pattern of AlN film. (b) (0002) plane XRC of AlN film.

force microscopy (AFM) (Bruker Multimode-8) were used to investigate the optical, structural, and surface morphological properties of the AlN film. The current–voltage (I – V) properties and time-dependent photocurrent (I – t) properties of the device were measured using semiconductor device analyzer (Agilent B1500A), 185-nm lamp (ZW21D15W/Y), and microprobe hot platform (KT-Z1000MR4T) under different temperatures. The measurements of temporal-dependent responses were performed by an ArF excimer laser (CL-5100, 193 nm) and a digital oscilloscope (Tektronix DPO 5104).

III. RESULTS AND DISCUSSION

AlN film growth process was studied using in situ RHEED, as shown in Fig. 1(a). A well-defined bright and long diffraction fringe can be observed in the RHEED pattern from AlN epitaxial film, suggesting a 2-D growth mode with a smooth surface morphology. To further evaluate the crystal quality of AlN film, HRXRD measurements were taken in this work. Fig. 1(b) shows the X-ray rocking curve (XRC) scan results of the (0002) plane of the AlN film with a full width at half peak (FWHM) value of 160.2 arcsec. Generally, the FWHM of the (0002) plane XRC peak can be used to estimate the screw dislocation density for AlN by the following formula [33]: $\rho_s = \beta_{(0002)}^2 / (4.35 \cdot |b_c|^2)$, where ρ_s is the screw dislocation density, $\beta_{(0002)}$ is the FWHM of the (0002) plane, and b_c stands for the Burgers vectors of the *c*-axial lattice constants of the AlN ($b_c = 0.4978$ nm). The screw dislocation density of our AlN thin film in this work was calculated to be 5.9×10^7 cm⁻².

Fig. 2(a) shows the room temperature Raman spectroscopy of AlN film with 532 nm laser excitation. The peak located at 657 cm⁻¹ can be assigned to E_2 (high) mode of AlN and the E_g mode peak of sapphire at 751 cm⁻¹ is used for wavenumber calibration. Interestingly, the position of E_2 (high) peak is highly sensitive to the stress in AlN [34], and the residual stress (σ) in AlN film can be evaluated from the shift of Raman peak position: $\sigma = \Delta\omega E_2 / k$, where $\Delta\omega E_2$ is the difference of E_2 (high) mode Raman shift between stressed and unstressed AlN samples and k is the stress coefficient of AlN. According to the previous reports, the values of $\Delta\omega E_2$ and k are 657.4 cm⁻¹ and 2.4 cm⁻¹GPa⁻¹ for freestanding AlN, respectively [34], [35], [36]. Therefore, the stress in our AlN thin film is calculated to be ~ 0.15 GPa. The optical transmission spectrum of the sample is shown in Fig. 2(b). The average transmittance of the grown AlN film is over 90% in the wavelength range of 210–700 nm. The bandgap of AlN

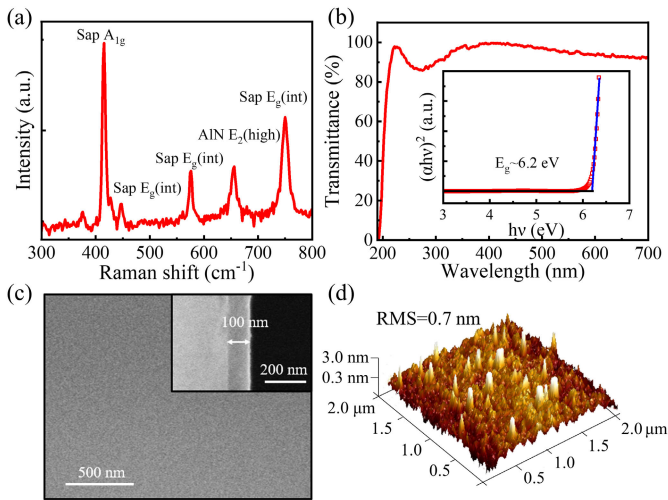


Fig. 2. (a) Raman spectrum of AlN thin film. (b) Absorption spectrum of AlN film in the 190–700 nm wavelength range at room temperature. The inset shows the variation of $(\alpha h\nu)^2$ versus the photoenergy ($h\nu$). (c) SEM and (d) AFM images of AlN thin film on $c\text{-Al}_2\text{O}_3$.

film is determined to be about 6.2 eV by Tauc plot in the inset of Fig. 2(b). The optical transmission results indicate that AlN thin film is very suitable for intrinsic VUV detection.

The top-view and cross-sectional SEM images of AlN thin film are shown in Fig. 2(c), and it can be found that the thickness of the AlN film is only about 100 nm with a uniform and smooth surface. Fig. 2(d) presents the AFM image of AlN film. A root mean square roughness (RMS) of 0.7 nm can be clearly observed within the $4 \mu\text{m}^2$ scanning area, suggesting a very flat surface of AlN film.

To investigate the VUV photodetection property of AlN thin film, a Pt–AlN–Pt photodetector has been demonstrated with interdigital Pt electrodes (500 μm long, 10 μm width, and 10 μm gap). In addition, a system consisting of a small vacuum chamber (~ 1 Pa) and a heating platform (25 $^\circ\text{C}$ –500 $^\circ\text{C}$) was used to study the performance of the device in high-temperature environment, as shown in Fig. 3(a). The I – V characteristic curves of the device in the dark and under 185-nm illumination were measured at different temperatures, as shown in Fig. 3(b) and (c), respectively. When the temperature is below 200 $^\circ\text{C}$, the dark current of the device is only about tens of femtoamperes at 20 V. As the temperature rises from 200 $^\circ\text{C}$ to 500 $^\circ\text{C}$, the dark current increases rapidly, and it can reach 218 pA at 500 $^\circ\text{C}$ (20 V). Moreover, under 185-nm irradiation (the optical power density: $\sim 35 \mu\text{W}/\text{cm}^2$), the current of the device shows a slight increase from 5.3 to 12 nA with the temperature increasing from 25 $^\circ\text{C}$ to 500 $^\circ\text{C}$ at 20 V. The increase in the semiconductor absorption coefficient may be the reason for the larger light current of the device at higher temperature [10], [37], [38], [39]. In addition, the I – t characteristics of the device were tested by periodically switching ON/OFF the 185 nm lamp at different temperatures at 20 V. As shown in Fig. 3(d), the periodic photoresponse of the device has excellent stability and repeatability at all temperatures. Even at high temperature of 500 $^\circ\text{C}$, the device still has a reliable and sensitive response to VUV light.

Responsivity (R) is an important parameter for describing the photoelectric conversion ability of a device, which is

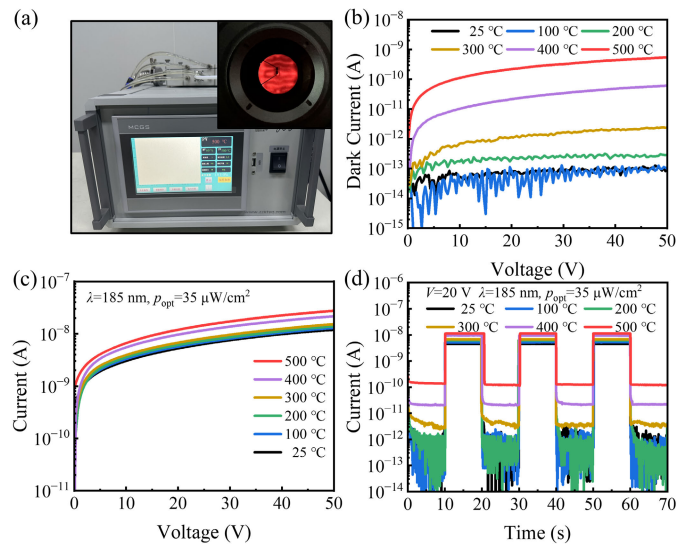


Fig. 3. (a) Variable-high-temperature photoresponse measurement system. (b) I – t characteristics of the device under 185 nm illumination at different temperatures. (c) I – V characteristics of the device in the dark state at different temperatures. (d) Time-dependent photocurrent of the device under the illumination of 185 nm light at different temperatures.

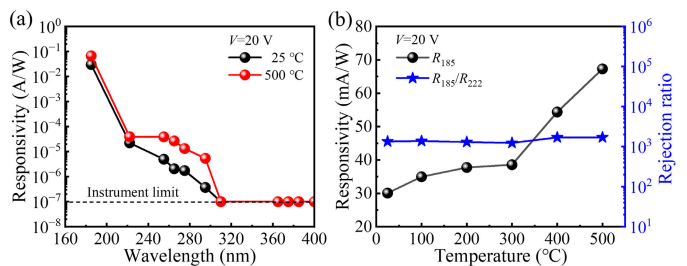


Fig. 4. (a) Responsivity of the device as a function of wavelength at different temperatures under 20 V bias. (b) Responsivity at 185 nm and rejection ratio (R_{185}/R_{222}) of the device as a function of temperature under 20 V bias.

expressed by the formula as [40]: $R = (I_{\text{light}} - I_{\text{dark}})/(p_{\text{opt}} \cdot S)$, where I_{light} is the current under illumination, I_{dark} is the dark current, p_{opt} is the illumination intensity, and S is the efficient area. Fig. 4(a) presents the dependence of the responsivity on the wavelength of the incident light at 25 $^\circ\text{C}$ and 500 $^\circ\text{C}$. The device has the maximum responsivity at 185 nm with a VUV/UVB (R_{185}/R_{222}) rejection ratio of over 10^3 at both 25 $^\circ\text{C}$ and 500 $^\circ\text{C}$, indicating the excellent intrinsic VUV spectral selectivity. The responsivities under 185 nm light irradiation at 25 $^\circ\text{C}$ and 500 $^\circ\text{C}$ are 30 and 67.3 mA/W, respectively. It should be mentioned here that the responsivity of the device to light with wavelengths greater than 310 nm is lower than the instrument limit of $\sim 1 \times 10^{-7}$ A/W, which means the VUV/UVB (R_{185}/R_{310}) rejection ratio is higher than 10^5 . Notably, as the temperature increases from 25 $^\circ\text{C}$ to 500 $^\circ\text{C}$, the responsivity of the device increases obviously, while the VUV/VUC (R_{185}/R_{222}) rejection ratio remains almost unchanged, as shown in Fig. 4(b).

To further investigate the response speed of the device, the temporal-dependent response of the AlN photodetector was tested using a pulsed ArF excimer laser with a wavelength of 193 nm (a laser pulsewidth of 10 ns and a frequency of 100 Hz). The response time is defined as the time interval between the amplitude of 90% and 10%. As shown in

TABLE I
COMPARISON TABLE FOR PERFORMANCE PARAMETERS OF VUV PHOTODETECTORS BASED ON AlN SINGLE-CRYSTALLINE FILMS

	Thickness	Buffer layer	Operating Temperature	Dark current (A)	Responsivity (mA/W)	Rejection ratio	90-10% Decay time (s)	Ref.
AlN	1.5 μm	AlN buffer	25 $^{\circ}\text{C}$	1×10^{-14} (100 V)	400@200 nm	$>10^4$ (R_{200}/R_{400})	-	[20]
AlN	500 nm	AlN/GaN buffer	25 $^{\circ}\text{C}$	2×10^{-14} (10 V)	80@202 nm	$>10^2$ (R_{202}/R_{213}) $>10^3$ (R_{202}/R_{285})	-	[21]
AlN	1.06 μm	AlN buffer	25 $^{\circ}\text{C}$ 100 $^{\circ}\text{C}$	2×10^{-13} (15 V) 2×10^{-12} (15 V)	1.4@202 nm -	$>10^2$ (R_{202}/R_{254}) -	>50 -	[24]
AlN	6 μm	AlN buffer	25 $^{\circ}\text{C}$	5×10^{-14} (10 V)	6.44@185 nm	-	3.6	[26]
AlN	1.5 μm	AlN buffer	25 $^{\circ}\text{C}$	1.3×10^{-14} (30 V)	6.8@170 nm	$>10^2$ (R_{200}/R_{240}) $>10^4$ (R_{200}/R_{360})	<3	[41]
AlN	1.5 μm	Without	25 $^{\circ}\text{C}$	6×10^{-12} (8 V)	10@200 nm	-	$<8 \times 10^{-3}$	[42]
AlN	100 nm	Without	25 $^{\circ}\text{C}$ 500 $^{\circ}\text{C}$	4×10^{-14} (20 V) 2×10^{-10} (20 V)	30@185 nm 67@185 nm	$>10^3$ (R_{185}/R_{222}) $>10^5$ (R_{185}/R_{310}) $>10^3$ (R_{185}/R_{222}) $>10^5$ (R_{185}/R_{310})	9×10^{-7} 9×10^{-7}	This work

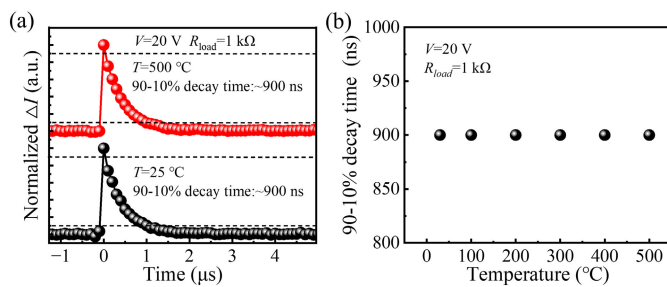


Fig. 5. (a) Transient photo-response upon a 193 nm pulsed laser excitation. (b) 90%–10% decay time of the device at different operating temperatures.

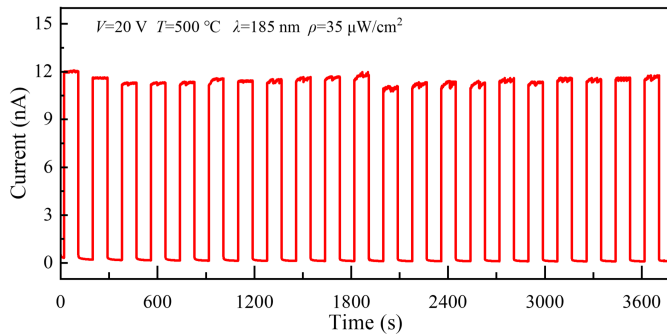


Fig. 6. Time-dependent photocurrent of the device under the illumination of 185 nm light at 500 $^{\circ}\text{C}$.

Fig. 5(a), the 90%–10% decay time of the device is as short as around 900 ns both at 25 $^{\circ}\text{C}$ and 500 $^{\circ}\text{C}$ with a load resistance (R_{load}) of 1 k Ω , which is much quicker than the most reported VUV photodetectors [20], [21], [26], [41], [43]. Fig. 5(b) shows the temperature dependence of the 90%–10% decay time of the device. It can be clearly observed that with increasing the operating temperature, the response speed of this AlN MSM VUV photodetector is almost unchanged.

Long-term stability at high temperature is also extremely critical for the practical application of a photodetector. As shown in Fig. 6, at 500 $^{\circ}\text{C}$, the photoelectric response characteristics of AlN VUV photodetector did not show any change after 3600 s, indicating that the device can work stably for a long time in a high-temperature environment.

Table I summarizes the key parameters of the reported VUV photodetectors based in AlN single-crystalline films. It can

be seen that our AlN thin-film device without any buffer layer exhibits the largest VUV/UVC rejection ratio and the highest operating temperature among the reported AlN VUV photodetectors. In addition, the dark current, responsivity, and response speed of our device are comparable with the best values obtained for AlN-based VUV photodetectors. More importantly, with increasing the operating temperature, the main performance of our AlN detector does not exhibit significant degradation. Even at high temperatures of 500 $^{\circ}\text{C}$, the device still shows excellent detection capabilities, and the main reason for these super VUV photodetection performance in this work (such as low dark current, large VUV/UVC rejection ratio, quick response speed, and high operating temperature) should be associated with the absence of poor-quality buffer layer and the relatively low defect density in AlN thin film.

IV. CONCLUSION

In summary, 100-nm-thick AlN thin film was prepared on fully nitride *c*-Al₂O₃ substrate using MBE without any buffer, and a low screw dislocation defect density of $\sim 5.9 \times 10^7$ cm⁻² can be estimated by XRC result. The Pt–AlN–Pt MSM photodetector was demonstrated and investigated at various operating temperatures. At 25 $^{\circ}\text{C}$, the device shows an ultralow dark current of ~ 40 fA and a high responsivity of 30 mA/W at 20 V. As the temperature rises to 500 $^{\circ}\text{C}$, the dark current of the device only increases to 218 pA, while the responsivity increases to 67.3 mA/W. In addition, the device has excellent repeatability and stability, and no obvious degradation can be observed in the VUV/UVC rejection ratio ($\sim 10^3$) and response speed (90%–10% decay time ~ 900 ns) with increasing the temperature from 25 $^{\circ}\text{C}$ to 500 $^{\circ}\text{C}$. The relatively high crystalline quality of AlN thin film and the absence of any buffer during the growth should be responsible for the excellent performance of our AlN VUV photodetector. Our findings in this work indicate that AlN materials have broad application prospects for VUV photodetection in harsh environments.

REFERENCES

- [1] D. N. Baker, S. G. Kanekal, X. Li, S. P. Monk, J. Goldstein, and J. L. Burch, "An extreme distortion of the Van Allen belt arising from the 'Halloween' solar storm in 2003," *Nature*, vol. 432, no. 7019, pp. 878–881, Dec. 2004, doi: 10.1038/nature03116.

- [2] D. F. P. Pile, "Vacuum-ultraviolet source," *Nature Photon.*, vol. 12, no. 10, p. 568, Sep. 2018, doi: [10.1038/s41566-018-0270-9](https://doi.org/10.1038/s41566-018-0270-9).
- [3] J. C. Kasper et al., "Alfvénic velocity spikes and rotational flows in the near-Sun solar wind," *Nature*, vol. 576, no. 7786, pp. 228–231, Dec. 2019, doi: [10.1038/s41586-019-1813-z](https://doi.org/10.1038/s41586-019-1813-z).
- [4] D. J. McComas et al., "Probing the energetic particle environment near the Sun," *Nature*, vol. 576, no. 7786, pp. 223–227, Dec. 2019, doi: [10.1038/s41586-019-1811-1](https://doi.org/10.1038/s41586-019-1811-1).
- [5] Q.-J. Peng et al., "DUV/VUV all-solid-state lasers: Twenty years of progress and the future," *IEEE J. Sel. Topics Quantum Electron.*, vol. 24, no. 5, pp. 1–12, Sep. 2018, doi: [10.1109/JSTQE.2018.2829665](https://doi.org/10.1109/JSTQE.2018.2829665).
- [6] G. Li, J. Zhang, and X. Hou, "Temperature dependence of performance of ZnO-based metal-semiconductor-metal ultraviolet photodetectors," *Sens. Actuators A, Phys.*, vol. 209, pp. 149–153, Mar. 2014, doi: [10.1016/j.sna.2014.01.029](https://doi.org/10.1016/j.sna.2014.01.029).
- [7] B. Zhao et al., "An ultrahigh responsivity (9.7 mA W^{-1}) self-powered solar-blind photodetector based on individual ZnO–Ga₂O₃ heterostructures," *Adv. Funct. Mater.*, vol. 27, no. 17, May 2017, Art. no. 1700264, doi: [10.1002/adfm.201700264](https://doi.org/10.1002/adfm.201700264).
- [8] Y. Chen, L. Su, M. Jiang, and X. Fang, "Switch type PANI/ZnO core-shell microwire heterojunction for UV photodetection," *J. Mater. Sci. Technol.*, vol. 105, pp. 259–265, Apr. 2022, doi: [10.1016/j.jmst.2021.07.031](https://doi.org/10.1016/j.jmst.2021.07.031).
- [9] J. Sun et al., "Suppression of persistent photoconductivity AlGaIn/GaN heterostructure photodetectors using pulsed heating," *Appl. Phys. Exp.*, vol. 12, no. 12, Nov. 2019, Art. no. 122007, doi: [10.7567/1882-0786/ab4f5b](https://doi.org/10.7567/1882-0786/ab4f5b).
- [10] X. Tang et al., "Temperature enhanced responsivity and speed in an AlGaIn/GaN metal-heterostructure-metal photodetector," *Appl. Phys. Lett.*, vol. 119, no. 1, Jul. 2021, Art. no. 013503, doi: [10.1063/5.0054612](https://doi.org/10.1063/5.0054612).
- [11] B. K. Pandey, T. N. Bhat, B. Roul, K. K. Nanda, and S. B. Krupanidhi, "BTO/GaN heterostructure based on Schottky junction for high-temperature selective ultra-violet photo detection," *J. Phys. D, Appl. Phys.*, vol. 51, no. 4, Jan. 2018, Art. no. 045104, doi: [10.1088/1361-6463/aa9f6b](https://doi.org/10.1088/1361-6463/aa9f6b).
- [12] S. Hou, P.-E. Hellstrom, C.-M. Zetterling, and M. Ostling, "550 °C 4H-SiC p-i-n photodiode array with two-layer metallization," *IEEE Electron Device Lett.*, vol. 37, no. 12, pp. 1594–1596, Dec. 2016, doi: [10.1109/LED.2016.2618122](https://doi.org/10.1109/LED.2016.2618122).
- [13] W.-C. Lien, D.-S. Tsai, D.-H. Lien, D. G. Senesky, J.-H. He, and A. P. Pisano, "4H-SiC metal-semiconductor-metal ultraviolet photodetectors in operation of 450 °C," *IEEE Electron Device Lett.*, vol. 33, no. 11, pp. 1586–1588, Nov. 2012, doi: [10.1109/LED.2012.2214759](https://doi.org/10.1109/LED.2012.2214759).
- [14] N. Watanabe, T. Kimoto, and J. Suda, "4H-SiC pn photodiodes with temperature-independent photoresponse up to 300 °C," *Appl. Phys. Exp.*, vol. 5, no. 9, Aug. 2012, Art. no. 094101, doi: [10.1143/APEX.5.094101](https://doi.org/10.1143/APEX.5.094101).
- [15] H.-T. Zhou et al., "High-performance high-temperature solar-blind photodetector based on polycrystalline Ga₂O₃ film," *J. Alloys Compounds*, vol. 847, Dec. 2020, Art. no. 156536, doi: [10.1016/j.jallcom.2020.156536](https://doi.org/10.1016/j.jallcom.2020.156536).
- [16] R. Zou et al., "High detectivity solar-blind high-temperature deep-ultraviolet photodetector based on multi-layered (100) facet-oriented β -Ga₂O₃ nanobelts," *Small*, vol. 10, no. 9, pp. 1848–1856, Feb. 2014, doi: [10.1002/sml.201302705](https://doi.org/10.1002/sml.201302705).
- [17] C. Lu et al., "A study for the influences of temperatures on ZnGa₂O₄ films and solar-blind sensing performances," *J. Phys. D, Appl. Phys.*, vol. 54, no. 40, Jul. 2021, Art. no. 405107, doi: [10.1088/1361-6463/ac1465](https://doi.org/10.1088/1361-6463/ac1465).
- [18] M. Liao, "Progress in semiconductor diamond photodetectors and MEMS sensors," *Funct. Diamond*, vol. 1, no. 1, pp. 29–46, Jan. 2021, doi: [10.1080/26941112.2021.1877019](https://doi.org/10.1080/26941112.2021.1877019).
- [19] Y. Taniyasu, M. Kasu, and T. Makimoto, "An aluminium nitride light-emitting diode with a wavelength of 210 nanometres," *Nature*, vol. 441, no. 7091, pp. 325–328, May 2006, doi: [10.1038/nature04760](https://doi.org/10.1038/nature04760).
- [20] J. Li, Z. Y. Fan, R. Dahal, M. L. Nakarmi, J. Y. Lin, and H. X. Jiang, "200 nm deep ultraviolet photodetectors based on AlN," *Appl. Phys. Lett.*, vol. 89, no. 21, Nov. 2006, Art. no. 213510, doi: [10.1063/1.2397021](https://doi.org/10.1063/1.2397021).
- [21] S. Nikishin et al., "High quality AlN for deep UV photodetectors," *Appl. Phys. Lett.*, vol. 95, no. 5, Aug. 2009, Art. no. 054101, doi: [10.1063/1.3200229](https://doi.org/10.1063/1.3200229).
- [22] W. Zheng, F. Huang, R. Zheng, and H. Wu, "Low-dimensional structure vacuum-ultraviolet-sensitive ($\lambda < 200 \text{ nm}$) photodetector with fast-response speed based on high-quality AlN micro/nanowire," *Adv. Mater.*, vol. 27, no. 26, pp. 3921–3927, May 2015, doi: [10.1002/adma.201500268](https://doi.org/10.1002/adma.201500268).
- [23] W. Wei et al., "Temperature dependence of stress and optical properties in AlN films grown by MOCVD," *Nanomaterials*, vol. 11, no. 3, p. 698, Mar. 2021, doi: [10.3390/nano11030698](https://doi.org/10.3390/nano11030698).
- [24] A. BenMoussa et al., "Developments, characterization and proton irradiation damage tests of AlN detectors for VUV solar observations," *Nucl. Instrum. Methods Phys. Res. Sect., Beam Interact. Mater. At.*, vol. 312, pp. 48–53, Oct. 2013, doi: [10.1016/j.nimb.2013.05.091](https://doi.org/10.1016/j.nimb.2013.05.091).
- [25] P. Zhang et al., "Vacuum ultraviolet photodetector with low dark current and fast response speed based on polycrystalline AlN thin film," *Phys. Status Solidi (RRL)-Rapid Res. Lett.*, vol. 17, no. 2, Feb. 2023, Art. no. 2200343, doi: [10.1002/pssr.202200343](https://doi.org/10.1002/pssr.202200343).
- [26] J. Yang et al., "Semipolar (11–22) AlN grown on *m*-plane sapphire by flow-rate modulation epitaxy for vacuum-ultraviolet photodetection," *Crystal Growth Design*, vol. 22, no. 3, pp. 1731–1737, Feb. 2022, doi: [10.1021/acs.cgd.1c01320](https://doi.org/10.1021/acs.cgd.1c01320).
- [27] D. V. Nechaev et al., "Effect of stoichiometric conditions and growth mode on threading dislocations filtering in AlN/c-Al₂O₃ templates grown by PA MBE," *Superlattices Microstruct.*, vol. 138, Feb. 2020, Art. no. 106368, doi: [10.1016/j.spmi.2019.106368](https://doi.org/10.1016/j.spmi.2019.106368).
- [28] D.-S. Tsai et al., "Solar-blind photodetectors for harsh electronics," *Sci. Rep.*, vol. 3, no. 1, pp. 1–5, Sep. 2013, doi: [10.1038/srep02628](https://doi.org/10.1038/srep02628).
- [29] T. Li et al., "In-plane enhanced epitaxy for step-flow AlN yielding a high-performance vacuum-ultraviolet photovoltaic detector," *CrystEng-Comm*, vol. 22, no. 4, pp. 654–659, Jan. 2020, doi: [10.1039/c9ce01852b](https://doi.org/10.1039/c9ce01852b).
- [30] L. Jia, T. Li, F. Huang, and W. Zheng, "Extremely high photovoltage (3.16 V) achieved in vacuum-ultraviolet-oriented van der Waals photovoltaics," *ACS Photon.*, vol. 9, no. 6, pp. 2101–2108, May 2022, doi: [10.1021/acsp Photonics.2c00342](https://doi.org/10.1021/acsp Photonics.2c00342).
- [31] M. Lee, M. Yang, H.-Y. Lee, H. U. Lee, H. Kim, and S. Park, "High crystalline aluminum nitride via highly enhanced adatom diffusion driven by point defect complex," *Appl. Surf. Sci.*, vol. 505, Mar. 2020, Art. no. 144615, doi: [10.1016/j.apsusc.2019.144615](https://doi.org/10.1016/j.apsusc.2019.144615).
- [32] X. Ni et al., "Improvement of AlN material quality by high-temperature annealing toward power diodes," *IEEE Trans. Electron Devices*, vol. 67, no. 10, pp. 3988–3991, Oct. 2020, doi: [10.1109/TED.2020.2991397](https://doi.org/10.1109/TED.2020.2991397).
- [33] S. R. Lee et al., "Effect of threading dislocations on the Bragg peak-widths of GaN, AlGaIn, and AlN heterolayers," *Appl. Phys. Lett.*, vol. 86, no. 24, Jun. 2005, Art. no. 241904, doi: [10.1063/1.1947367](https://doi.org/10.1063/1.1947367).
- [34] X. Rong et al., "Residual stress in AlN films grown on sapphire substrates by molecular beam epitaxy," *Superlattices Microstruct.*, vol. 93, pp. 27–31, May 2016, doi: [10.1016/j.spmi.2016.02.050](https://doi.org/10.1016/j.spmi.2016.02.050).
- [35] T. Prokofyeva et al., "Vibrational properties of AlN grown on (111)-oriented silicon," *Phys. Rev. B, Condens. Matter*, vol. 63, no. 12, Mar. 2001, doi: [10.1103/PhysRevB.63.125313](https://doi.org/10.1103/PhysRevB.63.125313).
- [36] V. Y. Davydov et al., "Phonon dispersion and Raman scattering in hexagonal GaN and AlN," *Phys. Rev. B, Condens. Matter*, vol. 58, no. 19, pp. 12899–12907, Nov. 1998, doi: [10.1103/PhysRevB.58.12899](https://doi.org/10.1103/PhysRevB.58.12899).
- [37] B. Chen et al., "Analysis of temperature-dependent characteristics of a 4H-SiC metal-semiconductor-metal ultraviolet photodetector," *Chin. Sci. Bull.*, vol. 57, no. 34, pp. 4427–4433, Dec. 2012, doi: [10.1007/s11434-012-5494-3](https://doi.org/10.1007/s11434-012-5494-3).
- [38] S. Sorifi, M. Moun, S. Kaushik, and R. Singh, "High-temperature performance of a GaSe nanosheet-based broadband photodetector," *ACS Appl. Electron. Mater.*, vol. 2, no. 3, pp. 670–676, Feb. 2020, doi: [10.1021/acsaelm.9b00770](https://doi.org/10.1021/acsaelm.9b00770).
- [39] S. Kaushik, S. Sorifi, and R. Singh, "Study of temperature dependent behavior of h-BN nanoflakes based deep UV photodetector," *Photon. Nanostruct.-Fundamentals Appl.*, vol. 43, Feb. 2021, Art. no. 100887, doi: [10.1016/j.photonics.2020.100887](https://doi.org/10.1016/j.photonics.2020.100887).
- [40] C. Li et al., "Ultrafast and broadband photodetectors based on a perovskite/organic bulk heterojunction for large-dynamic-range imaging," *Light, Sci. Appl.*, vol. 9, no. 1, p. 31, Mar. 2020, doi: [10.1038/s41377-020-0264-5](https://doi.org/10.1038/s41377-020-0264-5).
- [41] A. BenMoussa et al., "Characterization of AlN metal-semiconductor-metal diodes in the spectral range of 44–360 nm: Photoemission assessments," *Appl. Phys. Lett.*, vol. 92, no. 2, Jan. 2008, doi: [10.1063/1.2834701](https://doi.org/10.1063/1.2834701).
- [42] T. Li et al., "Three-dimensional metal-semiconductor-metal AlN deep-ultraviolet detector," *Opt. Lett.*, vol. 45, no. 12, pp. 3325–3328, Jun. 2020, doi: [10.1364/OL.394338](https://doi.org/10.1364/OL.394338).
- [43] S. Kaushik et al., "Surface modification of AlN using organic molecular layer for improved deep UV photodetector performance," *ACS Appl. Electron. Mater.*, vol. 2, no. 3, pp. 739–746, Mar. 2020, doi: [10.1021/acsaelm.9b00811](https://doi.org/10.1021/acsaelm.9b00811).